Recent Results from the three TRISTAN experiments

Ryosuke Itoh

Physics Division, KEK

Abstract

Recent results from the three TRISTAN experiments are presented. The measurements of the forward-backward asymmetry are reviewed. The results of QCD studies are discussed on the test of the existence of the triple gluon coupling and on the determination of $\Lambda_{\overline{MS}}$ using a new Monte Carlo. The various studies on the fragmentation are also presented.

1 Introduction

The TRISTAN electron-positron collider has been running since November 1986. The collision energy was gradually raised up from 50 GeV up to 64 GeV in 1989. The machine is currently running at 58 GeV to gain the luminosity.

Three groups, AMY, TOPAZ and VENUS, are taking data at TRISTAN. The integrated luminosity taken by now is about 50pb^{-1}/group which corresponds to about 7000 hadronic events. The results presented here are based on this data.

In the summer of 1990, the installation of micro-β magnets will be done in the accelerator. The luminosity is expected to be doubled after the installation. The experiments will be resumed from the beginning of 1991 and will continue for 3-4 years. The goal of the experiment is to obtain data with the luminosity of about 300pb^{-1} for detailed studies on the electro-weak theory and the QCD.

In this paper, I report the recent results from the TRISTAN experiments on three topics. The measurements of the forward-backward asymmetry are presented in section 2. Section 3 describes the studies on the QCD. The status of the studies on the fragmentation is given in section 4. The results are summarized in the last section.

2 Forward-backward Asymmetry

2.1 Introduction

The differential cross section of final state fermions produced in the e^+e^- annihilation can be written by the standard model in the form of

$$\frac{d\sigma}{d\cos\theta} = A_0(1+\cos^2\theta) + A_1\cos\theta \quad . \tag{1}$$

Since the second term is related to the contributions from the intermediating Z^0 and the interference between Z^0 and γ, the strength of Z^0 contribution can be measured by observing the forward-backward asymmetry of the produced fermions. The forward-backward asymmetry is defined as

$$A_{FB} = \frac{\int_0^{\pi/2}(d\sigma(\theta) - d\sigma(\pi-\theta))}{\sigma} = \frac{3}{8}\frac{A_1}{A_0} \quad . \tag{2}$$

The parameters A_0 and A_1 can be written using the vector and axial-vector coupling constants of electrons and fermions (v_e, v_f and a_e, a_f):

$$A_0 = Q_f^2 - Q_f v_e v_f \mathrm{Re}\{g(s)\} + \frac{1}{4}(v_e^2+a_e^2)(v_f^2+a_f^2)|g(s)|^2 \tag{3}$$

$$A_1 = -2Q_f a_e a_f \mathrm{Re}\{g(s)\} + \nu_e \nu_f a_e a_f |g(s)|^2 \tag{4}$$

where

$$g(s) = \frac{1}{8\sin^2\theta_W\cos^2\theta_W}\left(\frac{s}{s-M_Z^2+iM_Z\Gamma_Z}\right) \tag{5}$$

$$\nu_f = 2T_3 - 4Q_f\sin^2\theta_W \tag{6}$$

$$a_f = 2T_3 \quad . \tag{7}$$

T_3 is the third component of the weak isospin and Q_f is the electric charge of the fermion.

Figure 1 shows the forward-backward asymmetry as a function of $\sqrt{s}$ calculated using the formula above. Due to the difference in the charge of final state fermions, there are three types of asymmetries. As seen from the figure, the asymmetry becomes very large in the energy range of TRISTAN. In particular, the asymmetry of d-type quarks reaches its maximum in the energy range and therefore TRISTAN is a nice machine to study the asymmetry of b-quarks.

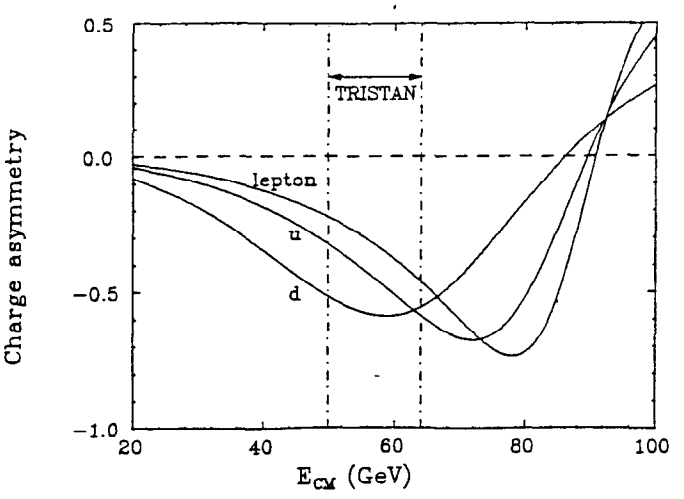

Figure 1: The forward-backward asymmetries of leptons, up and down type quarks calculated from the standard model as a function of the collision energy.

2.2 Leptons

The forward-backward asymmetry of leptons was measured for $e^+e^- \to \mu\bar{\mu}$ and $\tau\bar{\tau}$. Fig. 2 shows the differential cross sections of $\mu\bar{\mu}$ (a) and $\tau\bar{\tau}$ (b) measured by TOPAZ. The standard model predictions are also shown in solid lines. As seen, the measured data are consistent with the predictions.

The asymmetry was determined by fitting the measured differential cross section to formula 1. Fig. 3 shows the average value of the asymmetry measured by three TRISTAN experiments plotted as a function of $\sqrt{s}$. Also shown are the measurements by PEP and PETRA experiments[1]. All the measurements are well reproduced by the standard model predictions in both of $\mu\bar{\mu}$ and $\tau\bar{\tau}$ channels.

2.3 b-quarks

The forward-backward asymmetry of b-quarks is interesting at TRISTAN since the asymmetry becomes maximum at its energy range.

The b-quark events were identified by the leptons produced in the semi-

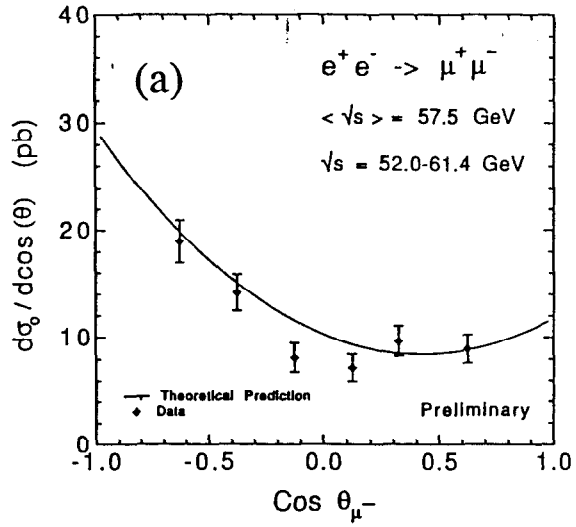

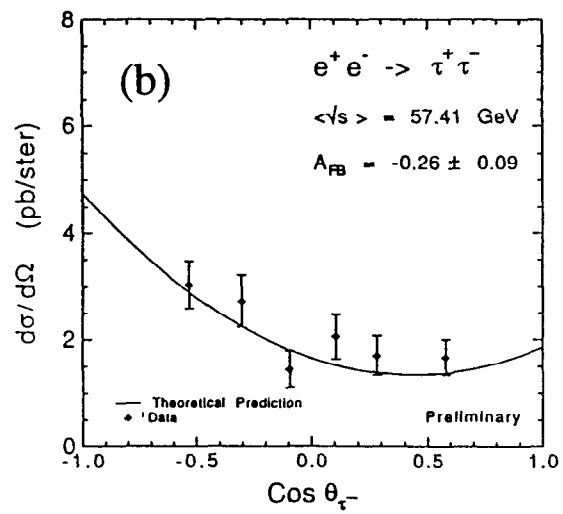

Figure 2: The differential cross sections of $\mu\bar{\mu}$ (a) and $\tau\bar{\tau}$ (b) measured by TOPAZ. Solid line shows the prediction by the standard model.

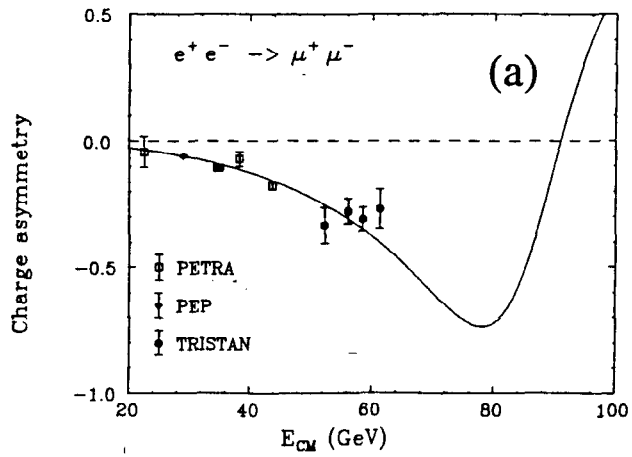

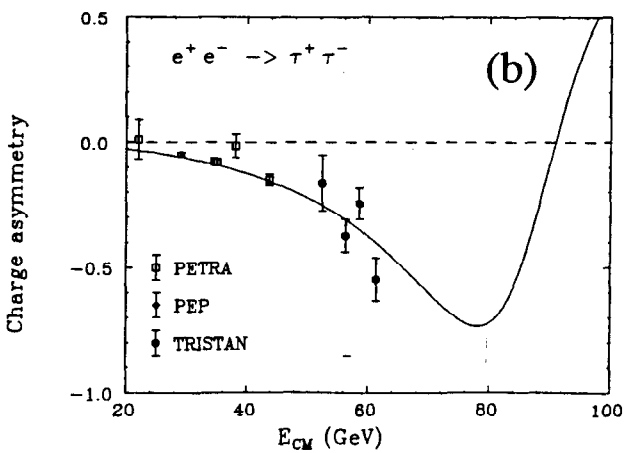

Figure 3: The measured forward-backward asymmetries of $\mu\bar{\mu}$ (a) and $\tau\bar{\tau}$ (b) averaged over the three TRISTAN experiments are plotted as a function of the collision energy. The measurements by other experiments are also plotted. The solid line shows the standard model prediction.

leptonic decay of b-quarks. AMY and TOPAZ identified only muons while VENUS used electrons also in addition to muons. The contamination of leptons from the decay of c-quarks and from the cascade-decay of b-quarks was estimated using the Monte Carlo and subtracted from the data. Fig. 4 shows the p_t distribution for inclusive muons by AMY. As seen, the distribution is well reproduced by the Monte Carlo.

The thrust axis of the event was defined as the direction of the primary b-quarks. The charge of the quark was determined from the charge of the identified lepton. The differential cross section of b-quarks measured by TOPAZ and AMY is shown in Fig. 5. A large asymmetry can be observed from the figure. The asymmetry was determined in the same manner as for the leptons and obtained as

$$\begin{aligned} A_{FB} = \; & -0.82 \pm 0.25 \pm 0.14 \quad (\mathrm{AMY}, \sqrt{s} = 57.2\mathrm{GeV}) \\ & -0.54 \pm 0.13 \qquad (\mathrm{VENUS}, \sqrt{s} = 57.9\mathrm{GeV(e)}, 58.5\mathrm{GeV}(\mu)) \\ & -0.64 \pm 0.32 \pm 0.10 \quad (\mathrm{TOPAZ}, \sqrt{s} = 58.9\mathrm{GeV}) \end{aligned}$$

where the values are not corrected for the $B^0 - \overline{B^0}$ mixing effect.

Fig. 6 shows the obtained asymmetry plotted as a function of $\sqrt{s}$. Measurements by the other experiments including the recent L3 result[2] are also shown. Although the data are not corrected for the $B^0 - \overline{B^0}$ mixing effect, the standard model prediction shown in the solid line well reproduces the measurements over the energy range from PEP to LEP.

One interesting point of the asymmetry of b-quarks is that the observed asymmetry is affected by the $B^0 - \bar{B}^0$ mixing. Due to the mixing, negative (positive) charged prompt leptons can be produced not only from b ($\bar{b}$)-quark decays, but also from $\bar{b}$ (b) quark decays. Therefore, the observed asymmetry is reduced as

$$A_{OBS} = (1 - 2\chi) A_b \tag{8}$$

where A_b is the true asymmetry and χ is the a probability that a b-quark becomes a $\bar{b}$-quark through the $B^0 - \overline{B^0}$ mixing, which is related to the mixing parameter as follows

$$\chi = f_d \frac{r_d}{1 + r_d} + f_s \frac{r_s}{1 + r_s} \quad . \tag{9}$$

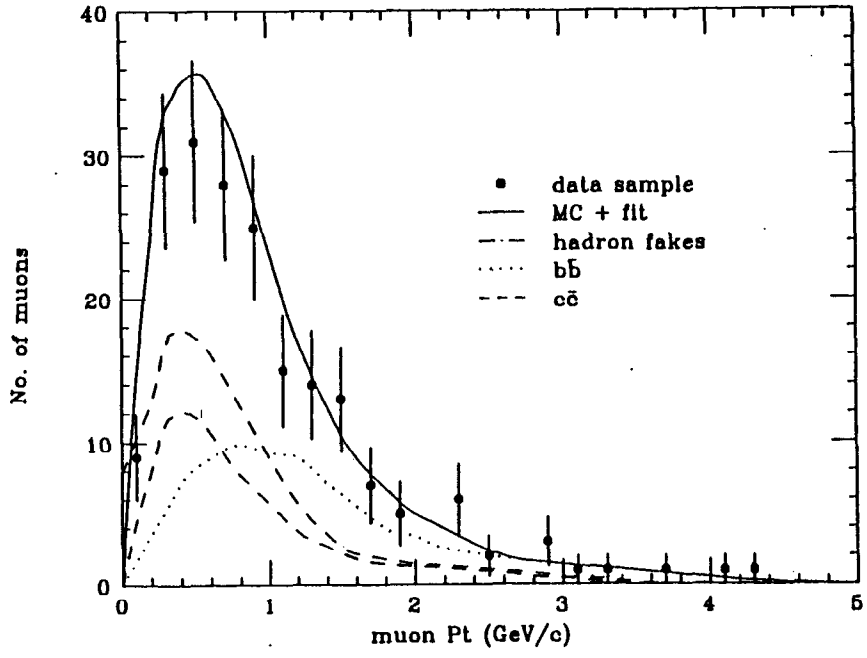

Figure 4: the p_t distribution of inclusive muons measured by AMY. The Monte Carlo predictions are also shown.

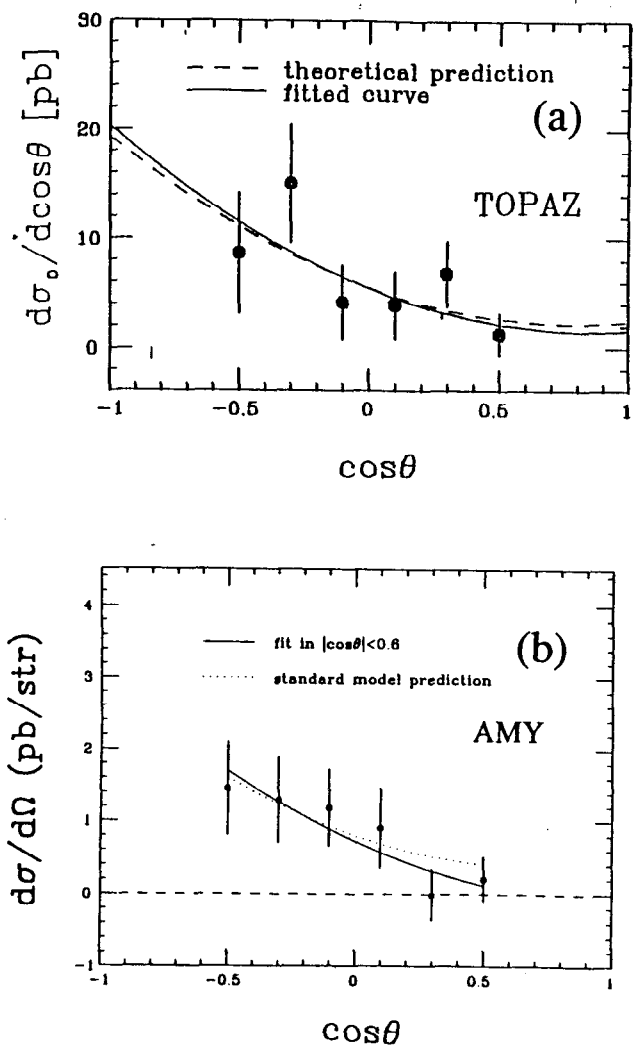

Figure 5: The differential cross section of $b\bar{b}$ measured by TOPAZ(a) and AMY(b). The solid line shows the fit to the data while the dotted line is the standard model prediction.

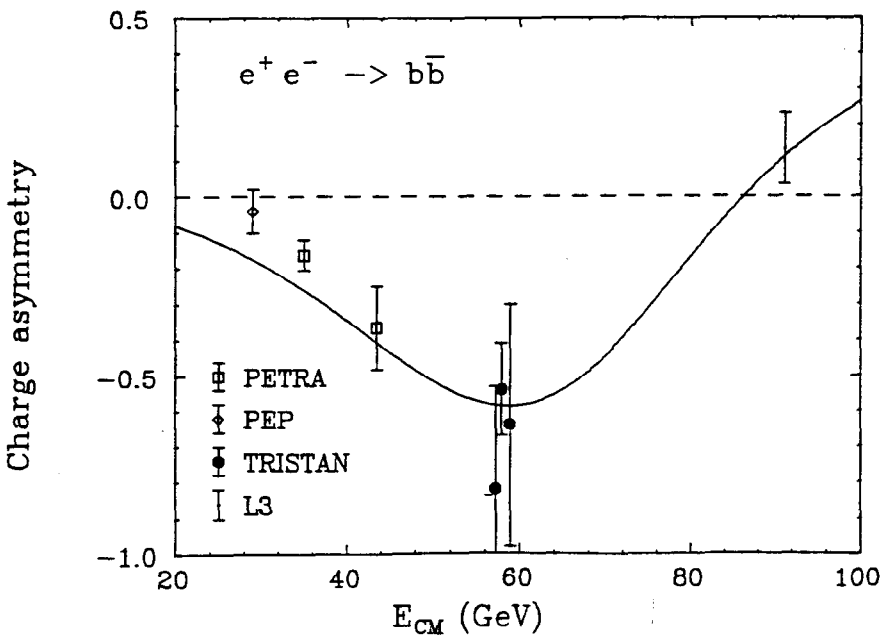

Figure 6: The measured asymmetry of b-quarks as a function of the collision energy. The measurements by the other experiments are also plotted. The solid line shows the standard model prediction where the effect of $B^0 - \overline{B^0}$ mixing is not taken into account.

f_d and f_s are the fractions of produced B_d and B_s bosons, respectively ($f_u + f_d + f_s = 1$). The parameter r_i is defined as

$$r_i = \frac{\Gamma(B_i^0 \to \overline{B_i^0} \to X')}{\Gamma(B_i^0 \to X)} \tag{10}$$

where i is one of d or s.

If the value of A_b is assumed to be the standard model value which is calculated using eq. 2, the value of the mixing parameter χ can be extracted by fitting the observed asymmetry to formula 8 with a free parameter χ. The measurements of the asymmetry of b-quarks by PEP, PETRA[6] and TRISTAN were combined and used for the fit. The value of χ was obtained from the fit as 0.131 ± 0.054. The χ was also measured using the di-lepton events by UA1[3], MAC[4] and Mark-II[5]. The value of χ averaged over all the measurements written above is $0.142^{+0.035}_{-0.031}$.

On the other hand, ARGUS[7] and CLEO[8] measured the mixing parameter of $B_d^0 - \overline{B_d^0}$ (r_d) from the decay of $\Upsilon(4s)$. The average of two measurements is 0.169 ± 0.038.

Using eq. 9, the mixing parameter r_s was estimated from the measured χ and r_d. The f_d and f_s in eq. 9 were assumed to be 0.375 and 0.15, respectively. Fig. 7 shows the 1σ range of measured χ and r_d plotted in the $r_s - r_d$ plane. As seen from the figure, r_s is likely to be 1. Fig. 8 shows the allowed region of r_s and r_d calculated from the measured χ and r_d. From this analysis, the hypothesis that the r_s is zero was excluded at 95% CL.

2.4 c-quarks

VENUS measured the forward-backward asymmetry of c-quarks by reconstructing D^*. The D^* first decays to D^0 and π, and then D^0 decays to K^- with one or more pions. VENUS reconstructed the decay channels of D^0 going to $K^-\pi^+$, $K^-\pi^+\pi^0$ and $K^-\pi^+\pi^+\pi^-$. Fig. 9 shows the mass difference between possible D^0s and D^* candidates. A mass peak of D^* decay is clearly seen.

The direction of the primary c-quark was determined from the direction of reconstructed D^* and the charge from the charge of D^*. The angular distribution of the reconstructed D^{*+} is shown in Fig. 10. Although the statistics is rather small, a large asymmetry can be observed. The value of the forward-

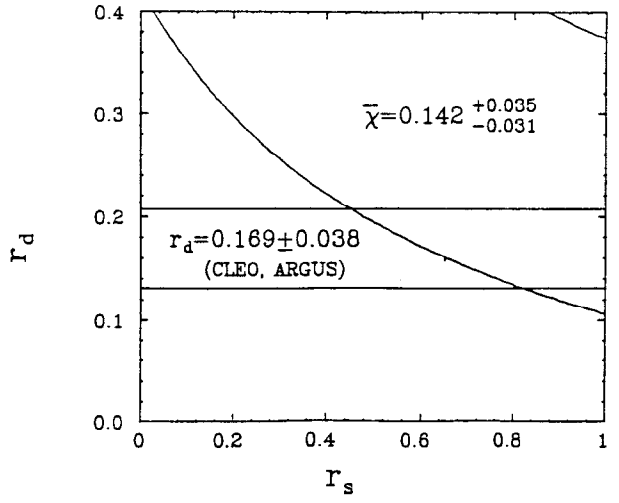

Figure 7: The 1σ regions of measured χ and r_d plotted in the $r_s - r_d$ plane.

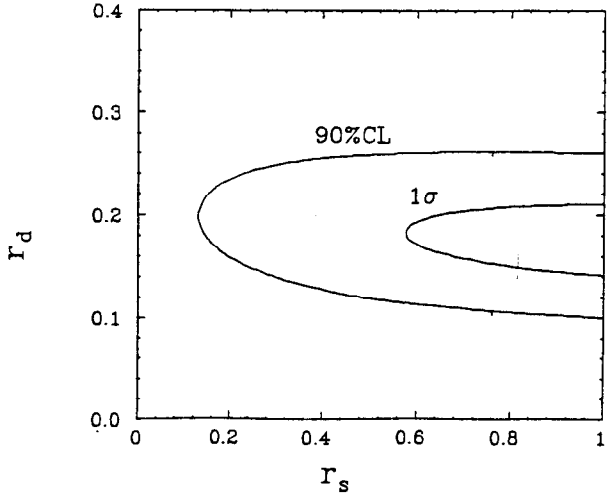

Figure 8: The allowed region in the $r_s - r_d$ plane.

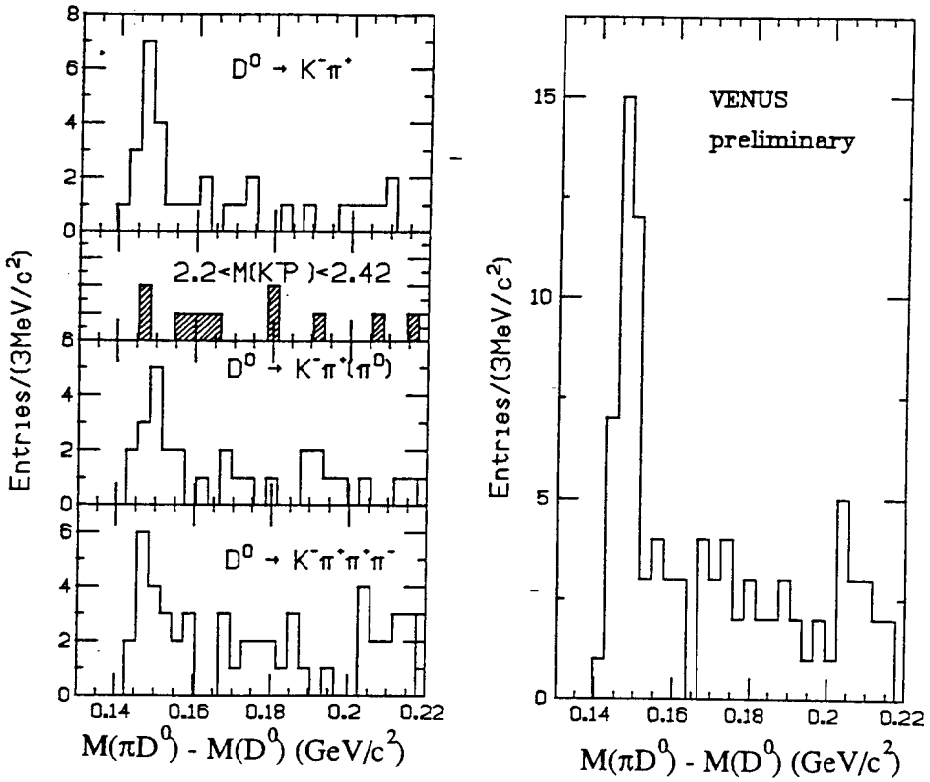

Figure 9: The mass difference between reconstructed D^0s and D^* candidates.

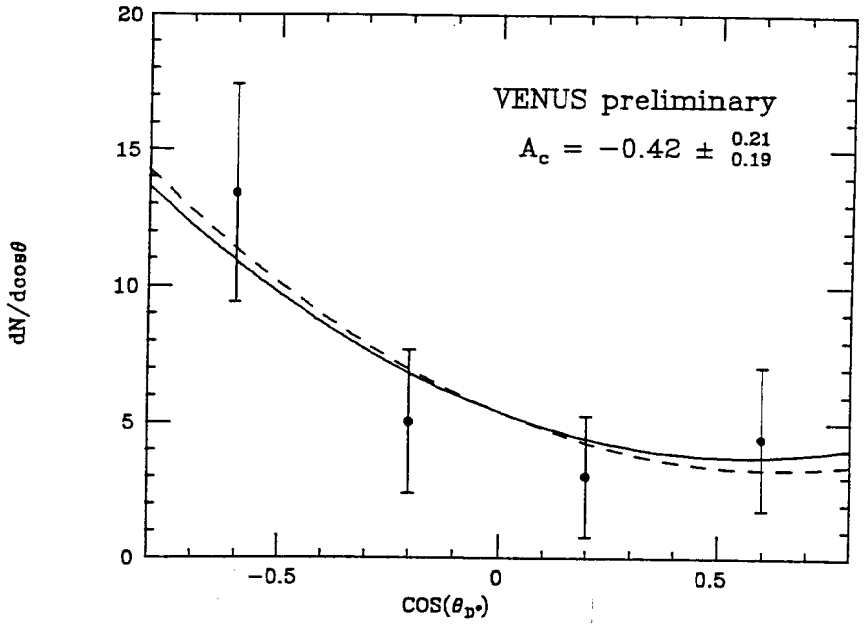

Figure 10: The angular distribution of D^{*+}. The solid line shows the fit to the data while the dashed line is the standard model prediction.

backward asymmetry of c-quarks was extracted from the angular distribution and obtained as $A_c = -0.42^{+0.21}_{-0.19}$.

2.5 Jets

The measurements of the forward-backward asymmetry of an individual quark flavor are onlypossible for heavy quarks and the statistics is limited due to the small efficiency in the identification of the heavy flavor. Alternatively, the forward-backward asymmetry of jets in the hadronic events was measured where the asymmetries of all five flavors are combined.

In the measurement of the asymmetry[9], the thrust axis of the event was defined as the direction of the primary quark. The charge of the primary quark was estimated from the charges of decay products. All the charged particles in the events were divided into two hemispheres along the thrust axis and the jet charge Q_{jet} was calculated for each hemisphere using

$$Q_{jet} = \sum_i q_i x_i^\alpha \qquad (11)$$

where q_i is the charge of i'th charged particle with i running over all the charged particles in the hemisphere. The x_i is the weighting factor. Some different parameters were chosen as this factor among three experiments. For example, TOPAZ used the rapidity with factor $\alpha = 0.8$ as the weighting factor. The charge of the primary quark was defined so that the jet with a larger Q_{jet} has a positive charge. Fig. 11 shows the differential cross section of jets measured by TOPAZ and VENUS.

The forward-backward asymmetry of jets was determined by fitting formula 1. The values obtained by three experiments were

$$\begin{aligned} A_{FB} = \; & 0.097 \pm 0.025 \pm 0.019 \quad (\mathrm{AMY}, \sqrt{s} = 57.2\mathrm{GeV}) \\ & 0.107 \pm 0.017 \pm 0.020 \quad (\mathrm{VENUS}, \sqrt{s} = 57.9\mathrm{GeV}) \\ & 0.091 \pm 0.022 \pm 0.016 \quad (\mathrm{TOPAZ}, \sqrt{s} = 58.1\mathrm{GeV}) \; . \end{aligned}$$

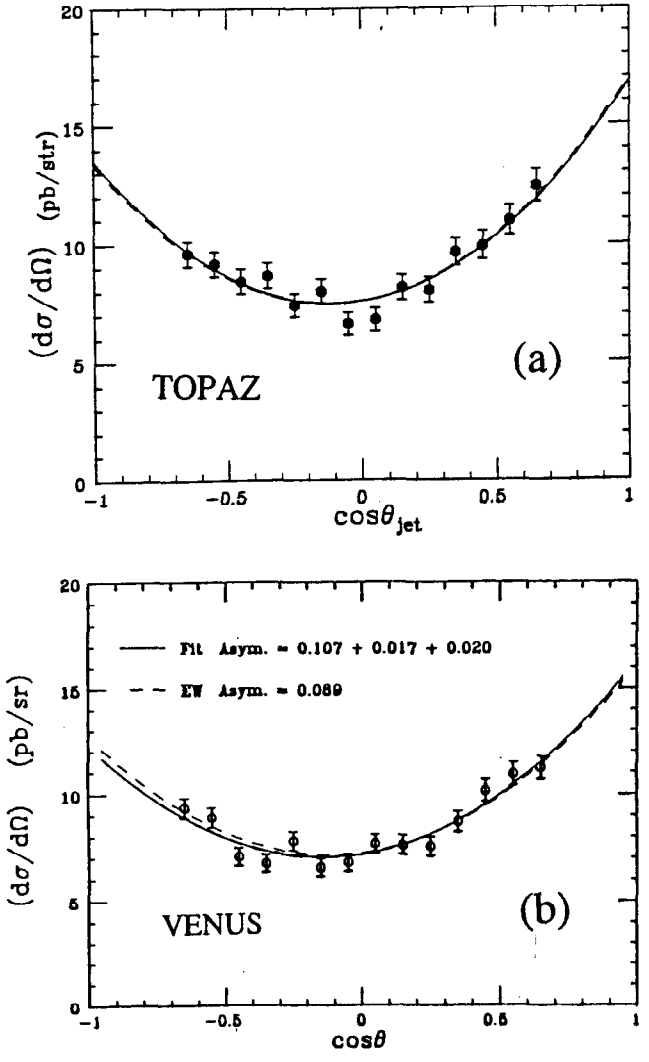

Figure 11: The differential cross section of jets measured by TOPAZ (a) and VENUS (b). The solid line shows the fit to the data while the dashed line is the standard model prediction.

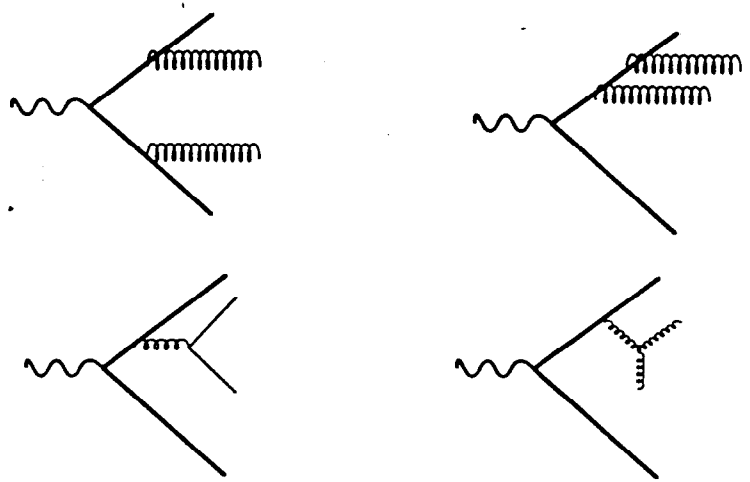

Figure 12: The diagrams of the 4-parton final states.

3 QCD

3.1 Triple Gluon Coupling

Since the QCD is based on the non-abelian gauge theory, the effect of the triple gluon coupling should be observed. In the e^+e^- annihilation, this effect can be observed in the 4-jet events. Fig. 12 shows the diagrams of the 4-parton final states. The triple gluon coupling is seen in the last diagram. Test of the existence of this vertex was difficult in the previous experiments since 4-jet events were not well resolved due to the large fragmentation effect. In the TRISTAN energy region, the fragmentation effect is relatively small and 4-jet events can be clearly distinguished. The existence of the triple gluon coupling was tested by the experiments at TRISTAN[10] for the first time.

When a quark emits a gluon in the bremsstrahlung process, the spin of the quark does not flip since the coupling between the quark and the gluon is the vector-coupling. Therefore, the spin component of the emitted gluon (g^*) is zero with respect to the direction of the quark. To conserve this spin component, the gluons split from this gluon ($g^* \to gg$) go preferably in parallel with the direction of the quark while the split quarks ($g^* \to qq$) go perpendicular to the direction. So the angular distribution of 4-jet events becomes different between the cases with and without the triple gluon coupling.

To study the angular distribution of 4-jet events, two observables were used by TRISTAN experiments. The first is the azimuthal angle χ_{BZ}[11] between the planes formed by jets1 and 2 and by jets3 and 4 where the jets are ordered according to their energies; $E_1 \geq E_2 \geq E_3 \geq E_4$. The jets1 and 2 are likely to be the primary quarks due to the bremsstrahlung character. Because of the spin conservation effect, the angle χ_{BZ} is relatively small for the events originated by the triple gluon vertex, while the angle becomes large for the events with split quarks.

The second is $cos\theta^*_{NR}$[12]. This observable is defined as

$$cos\theta^*_{NR} = \frac{|(\vec{p_1} - \vec{p_2}) \cdot (\vec{p_3} - \vec{p_4})|}{|\vec{p_1} - \vec{p_2}||\vec{p_3} - \vec{p_4}|} \tag{12}$$

where p_i is the momentum vector of i'th jet. This observable does not suffer from hard cuts which is required in χ_{BZ} and was used as a complementary observable to χ_{BZ}.

To select 4-jet events from the hadronic event sample, AMY and TOPAZ used the JADE clustering method[13] while VENUS used the Lund clustering[16]. In the JADE clustering, AMY set the cut-off in the scaled invariant mass of the jet (y_{cut}) at 0.024 while TOPAZ at 0.02. VENUS set the distance parameter of the Lund clustering (d_{join}) at 2.5 GeV. The numbers of selected 4-jet events are 139 by AMY, 157 by TOPAZ and 345 by VENUS.

In order to test the existence of the triple gluon vertices, the distributions of the observables were compared with the model predictions with and without triple gluon vertices (called the non-Abelian model and the Abelian model, respectively). AMY and VENUS obtained the model predictions using the Monte Carlo based on the QCD matrix element. AMY used the matrix calculated by F. Gutbrot et al. (GKS)[14] while VENUS used the calculation by R.K.Ellis et al. (ERT)[15]. These QCD matrix elements were combined with the Lund string fragmentation model[16]. The model predictions were obtained by turning on and off the triple gluon coupling term in the QCD matrix. On the other hand, TOPAZ compared the distributions of data directly

	non-Abelian model (QCD)	Abelian model
color factor (C_F)	$\frac{4}{3}$	1
gluon colors (N_C)	3	1
fraction of $q\bar{q}gg$	28.4%	65.5%
fraction of $q\bar{q}(g^* \rightarrow)Q\bar{Q}$	5.4%	34.5%
fraction of $q\bar{q}(g^* \rightarrow)gg$	66.2%	0%

Table 1: The difference between the non-Abelian and Abelian models. Values are from the model used by VENUS.

with the theoretical calculations by M.Bengtsson[12].

The differences between the Abelian and non-Abelian models are summarized in Table 1. In the Abelian model, the color factor is set to be 1 and the number of gluon colors to be 1. The fractions of the contributions of 4-jet diagrams in both models are also shown in the table.

In the TRISTAN experiments, the first result was obtained by AMY. Fig. 13 shows the distributions of χ_{BZ} and θ^*_{NR} measured by AMY. As seen, the data are consistent with the model in which triple gluon vertices are taken into account. From the θ^*_{NR} distribution, the Abelian model was excluded at 90% CL.

Since TOPAZ compared the data with the theoretical calculations directly, they checked that the calculation can reproduce the Monte Carlo data to justify the comparison. Fig. 14(a) shows the Monte Carlo data generated using the QCD matrix calculated by Gottshalk and Shatz[17]. Triple gluon vertices are taken into account in the matrix. The theoretical calculations with and without triple gluon vertices are also shown as histograms. As seen, the theoretical calculation with triple gluon vertices well reproduces the Monte Carlo data and the direct comparison is justified. The θ^*_{NR} distribution for the data of TOPAZ is shown in Fig. 14(b) plotted with the theoretical predictions. The distribution is consistent with the prediction with triple gluon vertices. The Abelian model was excluded at 95% CL.

VENUS also compared the distributions of χ_{BZ} and θ^*_{NR} with the model predictions as shown in Fig. 15. From the comparison, the Abelian model was excluded at 95% CL. They also obtained the model independent limit to the

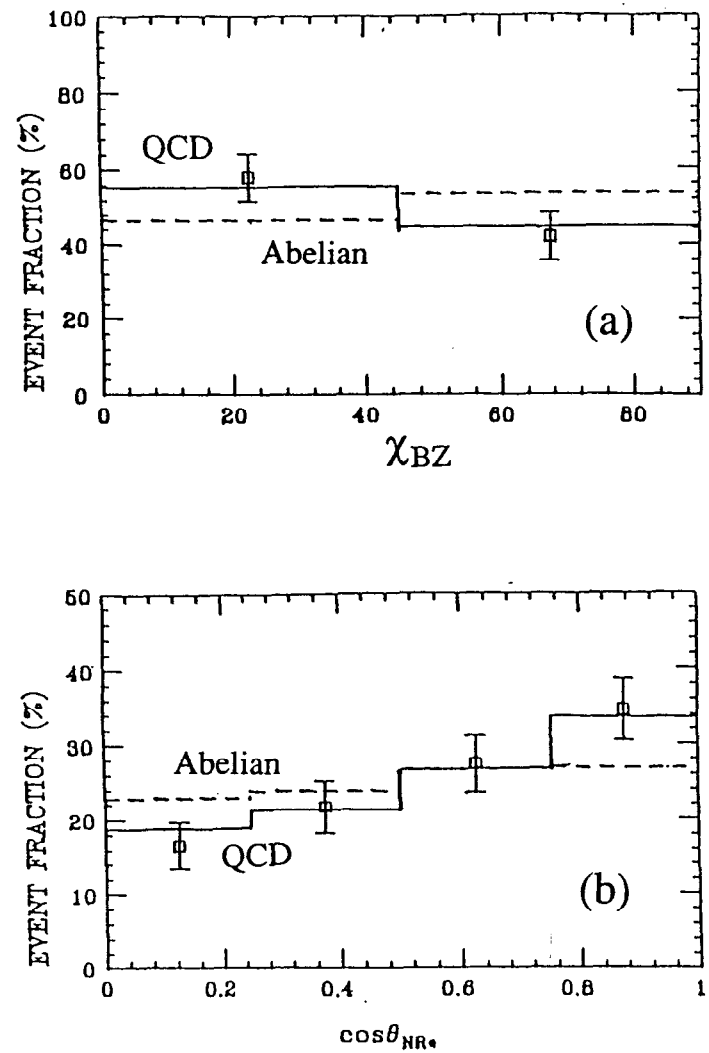

Figure 13: The distributions of χ_{BZ} (a) and θ^*_{NR} (b) measured by AMY. The Monte Carlo predictions with and without triple gluon vertices are shown in the solid and dashed lines, respectively.

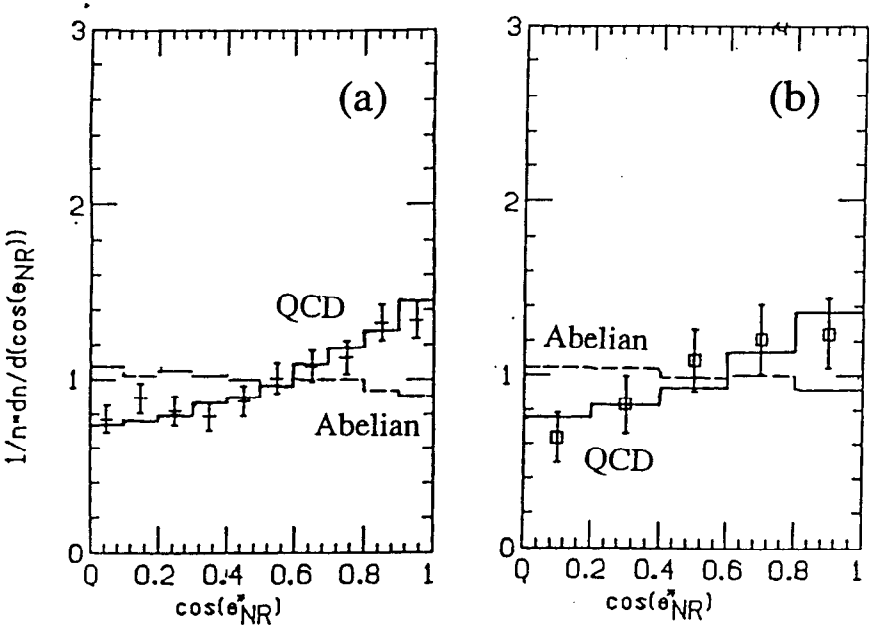

Figure 14: Fig.(a) shows the distribution of θ^*_{NR} for the Monte Carlo events while fig.(b) for the data obtained by TOPAZ. The theoretical predictions with and without triple gluon vertices are shown in the solid and dashed lines, respectively.

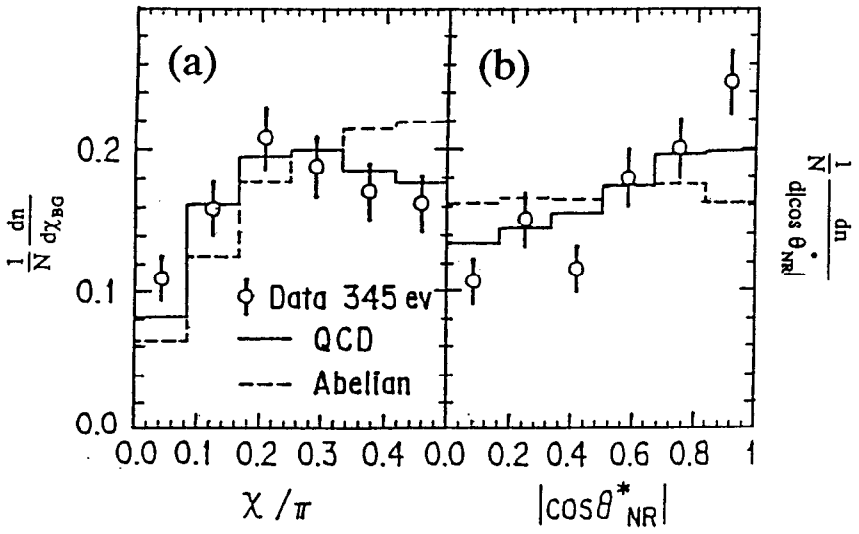

Figure 15: The distributions of χ_{BZ} (a) and θ^*_{NR} (b) measured by VENUS. The solid and dashed line shows the Monte Carlo predictions with and without triple gluon vertices.

fraction of each 4-jet diagram. In their model, the fractions are expressed as functions of the ratios N_c/C_F and T_R/C_F where N_c is number of gluon colors, C_F is the color factor and T_R is the flavor factor. The result is shown in Fig. 16.

In conclusion, the existence of the triple gluon coupling was confirmed and the model without triple gluon vertices was excluded at 95% confidence level by TRISTAN experiments.

3.2 Determination of $\Lambda_{\overline{MS}}$ Using NLL MC

To determine the $\Lambda_{\overline{MS}}$ in the e^+e^- annihilation, the Monte Carlo based on the QCD matrix element of order of α_s^2 has been used. The distributions of various event shape parameters are compared with the data and the value of α_s in the Monte Carlo is determined from the fit. The $\Lambda_{\overline{MS}}$ is derived from the determined value of α_s.

However, this method has several problems. Since the 4-jet cross section in second order has only contributions at the tree level, the Monte Carlo cannot reproduce the 4-jet cross sections of the data properly. Therefore, some corrections for this effect are necessary in the determination of α_s. The fragmentation dependence is another problem. In the Monte Carlo, the partons generated using the QCD matrix are converted into hadrons according to a certain fragmentation scheme. Since QCD matrix cannot produce more than 4 primary partons, the distribution of resulting hadrons has a large dependence on the fragmentation scheme. The translation from α_s into $\Lambda_{\overline{MS}}$ also has a theoretical difficulty since the energy-scale parameter μ in the relation between the $\Lambda_{\overline{MS}}$ and α_s is not well-defined.

The Monte Carlo based on the parton shower can be an answer to these problems. In the parton shower model, because of the iterative use of the Altarelli-Parisi splitting functions, the parton shower evolves with an unlimited number of partons until the Q^2 of the parton system becomes less than a cutoff value (typically $\sim 1GeV^2$) . Therefore the model can well reproduce the 4-jet cross sections and is relatively insensitive to the fragmentation scheme. For example, the Lund JETSET 6.3[16] is one of the widely-used Monte Carlo based on the parton shower.

However, the parton shower models currently being used are based on the leading-log approximation (LLA-PS)[18]. This approximation can be written

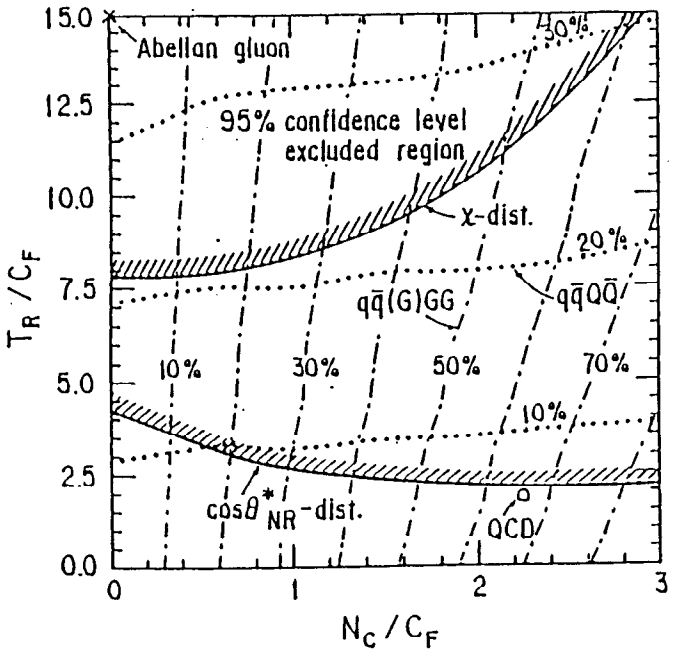

Figure 16: Experimental bounds on the fractions of 4-jet diagrams. The shaded area shows the excluded regions at 95% CL by χ_{BZ} and θ^*_{NR}.

in the form of

$$\sum_{n=0} c_n(\alpha_s log\frac{Q^2}{Q_0^2})^n \quad . \tag{13}$$

As seen, the second order coupling is not included in this approximation and the renormalization scheme cannot be specified. Therefore, $\Lambda_{\overline{MS}}$ cannot be defined in the LLA-PS.

Recently, the parton shower model was extended to the next-to-leading-log order (NLL-PS) by T.Munehisa and K.Kato[19]. The extension was done in the form of

$$\sum_{n=0} c_n(1 + d_n\alpha_s)(\alpha_s log\frac{Q^2}{Q_0^2})^n \tag{14}$$

where the second order coupling is included. Since the renormalization scheme can be specified in this approximation, the $\Lambda_{\overline{MS}}$ can be properly defined in the model. The determination of $\Lambda_{\overline{MS}}$ using this NLL parton shower model was done by all three experiments at TRISTAN[20].

The NLL-PS was combined with two fragmentation models to form a Monte Carlo (NLL Monte Carlo). One is the Lund string fragmentation[16] done by T.Kamae et al.[21] This was used by AMY and TOPAZ. The other is the EPOCS string fragmentation[22] done by T.Watanabe which was used by VENUS.

Fig. 17 shows the distributions of the momentum fraction and the thrust for the hadronic events of VENUS plotted with the predictions by the NLL Monte Carlo. The data are well reproduced by the Monte Carlo. Fig. 18 shows the P_T^{in} and P_T^{out} distributions of AMY. The predictions by various Monte Carlo simulations are also shown. As seen, the distributions are well described by the NLL Monte Carlo as well as the Lund JETSET 6.3.

The determination of $\Lambda_{\overline{MS}}$ was done by comparing the 3-jet fraction (R3). The JADE clustering was used to measure the R3 since the R3 becomes relatively insensitive to the fragmentation when the method is used[23]. Fig. 19 shows the fractions of 2, 3, 4 and 5 jet events by VENUS as functions of y_{cut} where y_{cut} is the cut-off parameter in the scaled invariant mass of the jet. In the figure, solid lines and dashed lines are the predictions with and without the fragmentation, respectively. The difference between these two predictions is small and the dependence on the fragmentation is confirmed to be negligible. Fig. 20 shows the values of $\Lambda_{\overline{MS}}$ determined by VENUS as a function of y_{cut}.

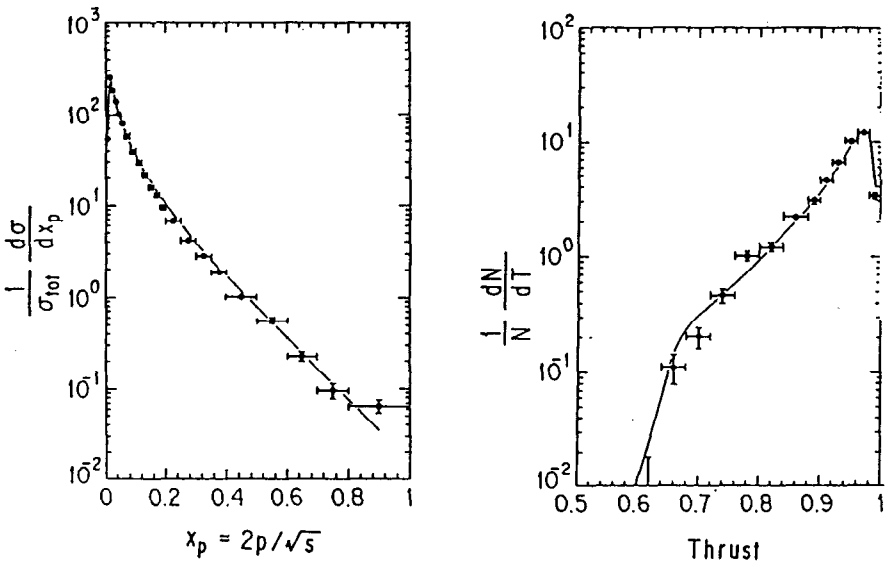

Figure 17: The distributions of the momentum fraction and the thrust measured by VENUS. The solid lines show the predictions of the NLL Monte Carlo.

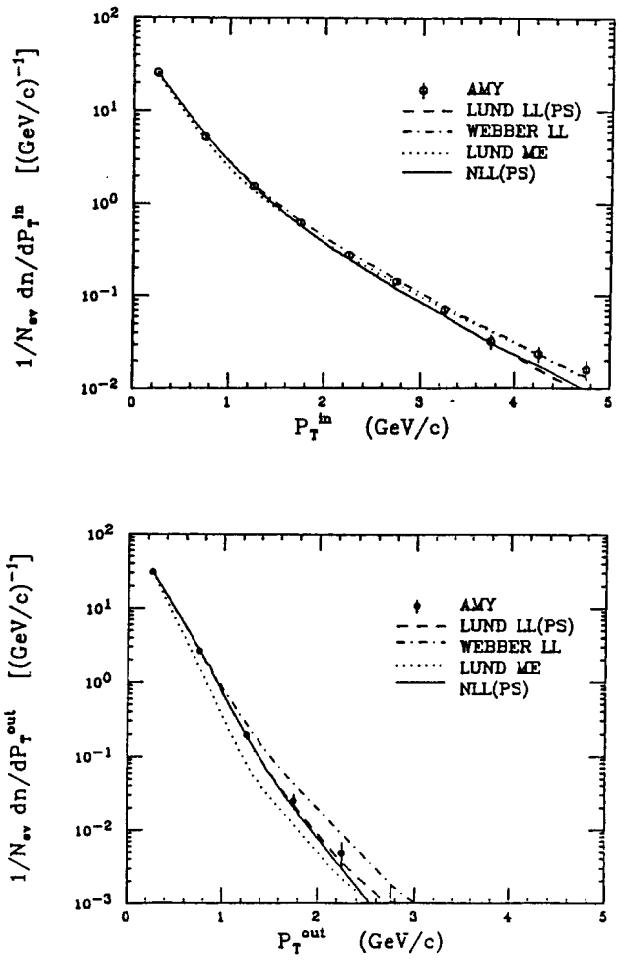

Figure 18: P_T^{in} and P_T^{out} distributions measured by AMY. Predictions by several Monte Carlo models are also shown.

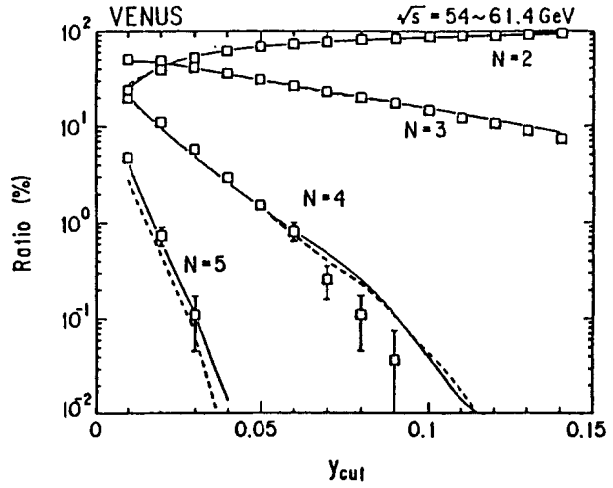

Figure 19: The fractions of 2,3,4 and 5 jet events measured by VENUS. The solid line shows the Monte Carlo prediction with the fragmentation while the dashed line without the fragmentation.

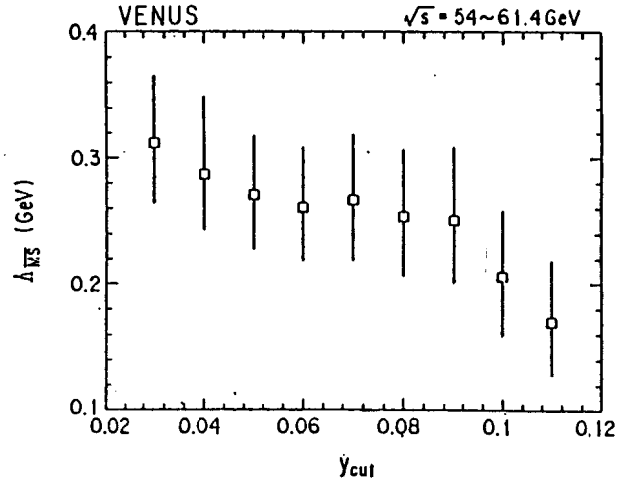

Figure 20: The values of $\Lambda_{\overline{MS}}$ determined by VENUS as a function of y_{cut}.

The determined $\Lambda_{\overline{MS}}$ is stable for the variation in y_{cut}.

In the determination of $\Lambda_{\overline{MS}}$, the R3 value at $y_{cut} = 0.08$ was used. The measured R3 was compared with Monte Carlo predictions with various $\Lambda_{\overline{MS}}$ values. The $\Lambda_{\overline{MS}}$ was determined from the value where the measured R3 is reproduced. The determined values by three groups are

$$\begin{aligned} \Lambda_{\overline{MS}} = \quad & 240 \pm 70 \pm 60 MeV \quad && \text{(AMY, Lund fragmentation)} \\ & 254^{+55}_{-47} \pm 56 MeV && \text{(VENUS, EPOCS frg.)} \\ & 232^{+23}_{-79}(stat. + sys.) MeV && \text{(TOPAZ, Lund frg.)} . \end{aligned}$$

4 Fragmentation

4.1 Heavy Quark Fragmentation

Since hadrons originated from heavy quarks carry a large fraction of original energy of the quarks, the fragmentation function of heavy quarks has a peak at large z where z is defined as

$$z = \frac{E_{hadron}}{E_{quark}} . \tag{15}$$

The average energy fraction $< z >$ of heavy-flavored hadrons can be given in the form of[24]

$$< z > \sim 1 - \frac{1\ GeV}{m_q} \tag{16}$$

where m_q is the mass of the heavy quark. From this formula, $< z >$ for the b-quark is expected to be larger than that for the c-quark.

AMY group estimated $< z >$ values for c and b quarks using the prompt leptons produced in the decay of heavy quarks. The longitudinal momentum component of the lepton reflects the momentum of the heavy hadron while the transverse component carries the information of the heavy quark flavor of the hadron. Therefore, from the simultaneous fit to the longitudinal and transverse momentum spectra of the prompt leptons, the $< z >$ values for c and b quarks can be estimated.

Although the measurement of the energy of the initial quarks is necessary to obtain the energy fraction z, the energy is not directly measurable. So AMY used x_E instead of z where x_E is defined as

$$x_E = \frac{E_{hadron}}{E_{beam}} . \tag{17}$$

The inclusive muon events were used in this analysis. The two dimensional distribution of the momentum and the transverse momentum (p, p_t) of muons was obtained for the events. The distribution was fitted by the expectation function parametrized as a function of fragmentation functions of c and b quarks. The Peterson function[25] was used as the fragmentation function which has the form of

$$f_Q(x) = \frac{N}{x(x - \frac{1}{x} - \frac{\epsilon_Q}{(1-x)})^2} . \tag{18}$$

Fig. 21 shows some of the results of the fit. From the fit, ϵ_c for c quarks and ϵ_b for b quarks were determined. Obtained values are

$$\begin{aligned} \epsilon_c &= 0.197^{+0.185}_{-0.095} \\ \epsilon_b &= 0.017^{+0.049}_{-0.013} . \end{aligned}$$

Using these values, $< x_E >$ for c and b quarks were estimated to be

$$\begin{aligned} < x_E >_c &= 0.57 \pm 0.06 \\ < x_E >_b &= 0.77^{+0.08}_{-0.10} . \end{aligned}$$

4.2 Inclusive Cross Sections of Charged Particles

The inclusive cross sections of $\pi^{\pm}$, $K^{\pm}$ and p, $\bar{p}$ in the e^+e^- annihilation are good measures to study the fragmentation model. VENUS and TOPAZ measured these cross sections at TRISTAN.

In the measurement by VENUS, the particle identification was done by measuring the time of flight (TOF) of the particle. Fig. 22 shows the result of VENUS. As seen from the figure, the Lund model[16] well reproduces the data in this region. Since the particle identification by TOF is limited to the momentum range less than $\sim$ 1GeV/c, their study is restricted to very low region of the energy fraction.

On the other hand, TOPAZ identified the particle species by the simultaneous measurements of the energy loss and the momentum of the particle

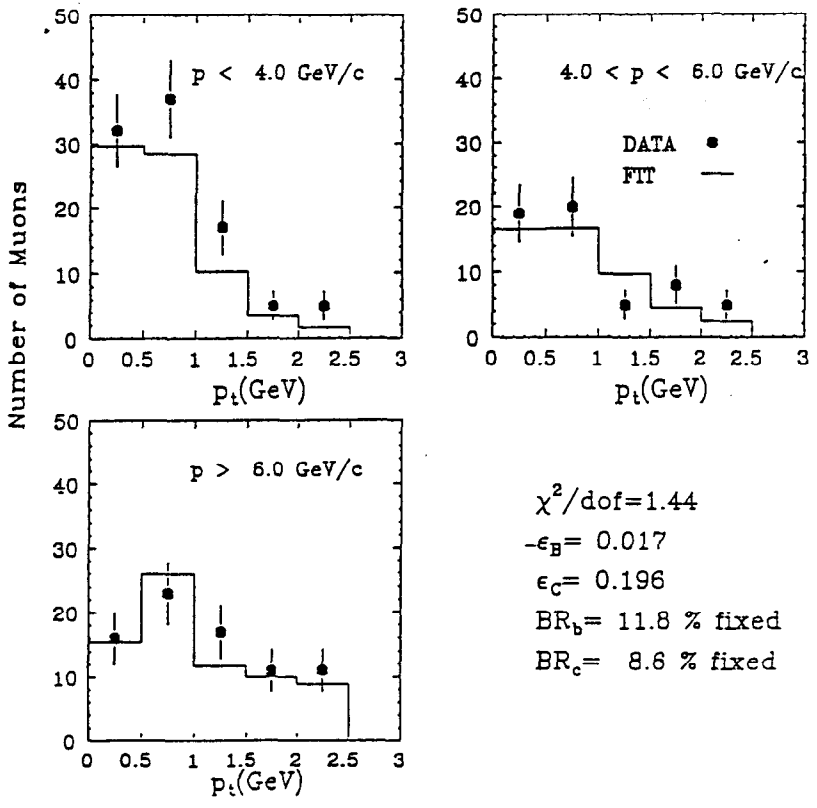

Figure 21: Results of the fit to the p and p_t of inclusive muons.

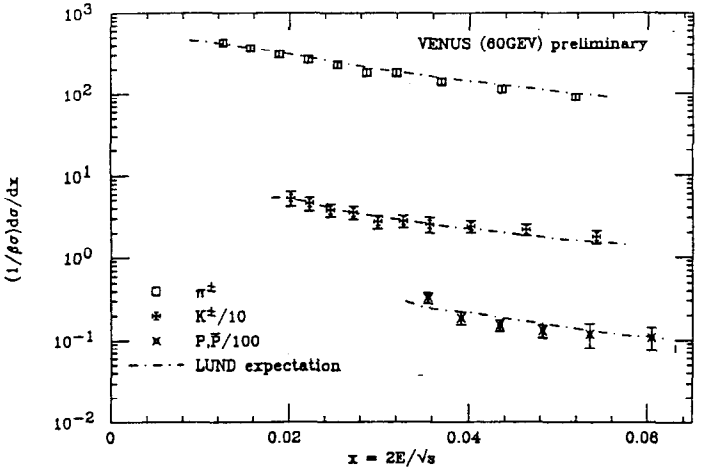

Figure 22: The inclusive cross sections of $\pi^{\pm}$, $K^{\pm}$ and $p, \bar{p}$ measured by VENUS as a function of the energy fraction of the particle. The predictions by the Lund Monte Carlo are also shown.

using the time projection chamber. Fig. 23 is the so-called TPC plot. As seen, pions, kaons and protons are clearly separated in the momentum region below 1 GeV/c. In the relativistic-rise region, statistical fits were done to obtain the number of each particle species. The dE/dx distribution in a momentum bin was fitted by the sum of gaussians corresponding to electrons, pions, kaons and protons. Fig. 24 shows an example of the statistical fit. The number of each particle species was calculated from the obtained parameters of the gaussian.

The measured cross sections are shown in Fig. 25 as a function of the momentum fraction. The data are consistent with the Lund predictions[16] in the measured range. However, the error bars are still large for kaons and protons with high momentum fractions and more statistics is necessary for further studies such as the study of the baryon production.

4.3 Bose-Einstein Correlation in Pion Production

Since pion obeys the Bose-Einstein statistics, the enhancement in the production of pions which have the same charge and the similar momentum should

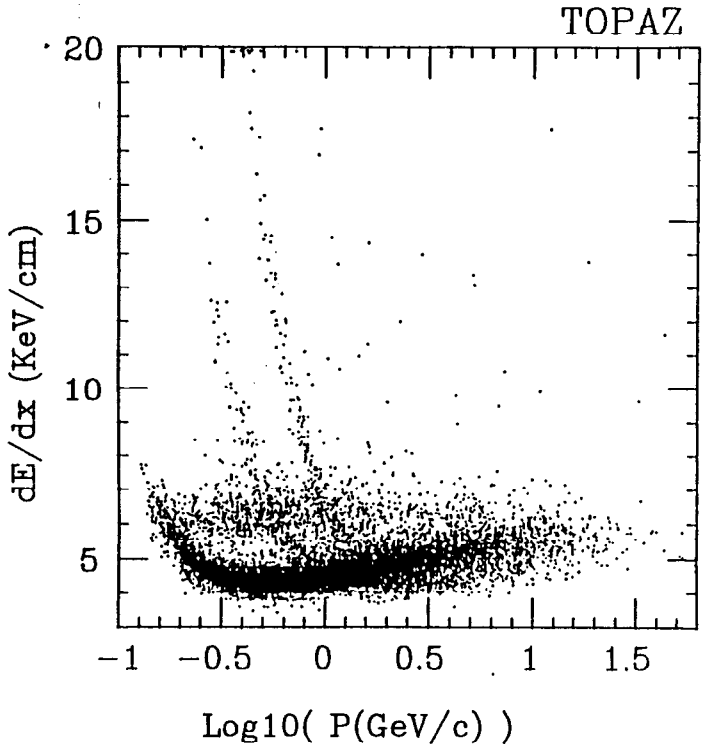

Figure 23: The dE/dx distribution as a function of the momentum measured by TOPAZ. This plot is called the "TPC-plot".

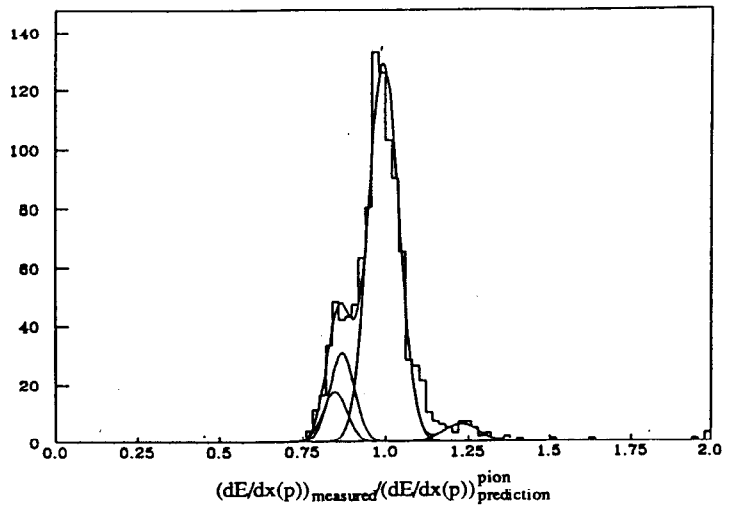

Figure 24: The result of the statistical fit to the dE/dx distribution in the momentum range from 2.62 GeV/c to 3.67GeV/c. The distribution is fitted by the sum of gaussians corresponding to electrons, pions, kaons and protons.

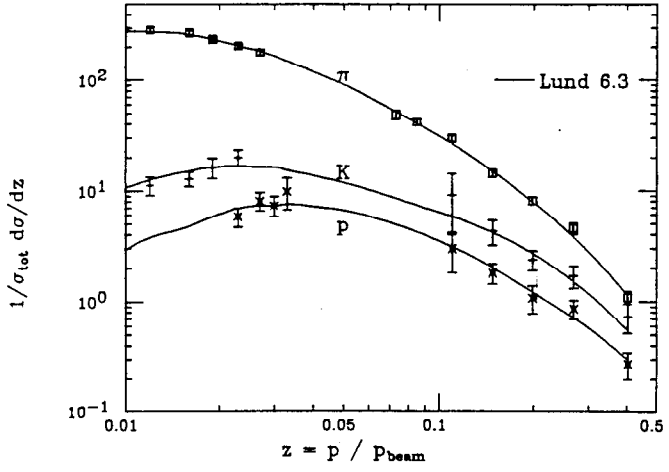

Figure 25: The inclusive cross sections of $\pi^{\pm}$, $K^{\pm}$ and $p, \bar{p}$ measured by TOPAZ as a function of the momentum fraction of the particle. The solid lines show the predictions by the Lund Monte Carlo.

be observed in the hadronic final states of e^+e^- annihilation (Goldhabor-Goldhabor-Lee-Pais (GGLP) effect)[26]. AMY studied this effect in the hadronic event sample.

Fig. 26 shows the ratio of the same and opposite charged particle pairs in the hadronic final states as a function of the square of the momentum difference in the particle pair (Q^2). The enhancement in the production of the same-charged particle pairs can be seen in the low Q^2 region.

The correlation effect was parametrized in the form of

$$R(Q^2) = N_0(1 + f_\pi(Q^2)\lambda e^{-R_0^2Q^2})(1 + \gamma Q^2) \ . \qquad (19)$$

$R(Q^2)$ is the ratio of the numbers of the same and opposite charged pion pairs. $f_\pi(Q^2)$ is the correction function for the contamination of kaons and protons estimated using the Monte Carlo. λ and R_0 are the parameters in the Bose-Einstein correlation function. λ stands for the strength of the correlation while R_0 means the average size of the source. N_0 is the normalization factor of the ratio and γ is the correction factor for the long range correlation.

By fitting the measured distribution to this function, the Bose-Einstein correlation parameters were obtained as

$$\begin{aligned} \lambda &= 0.60 \pm 0.13 \pm 0.08 \\ R_0 &= 1.18 \pm 0.17 \pm 0.10(fm) \ . \end{aligned}$$

5 Summary

- Charge asymmetries were measured for the final state $\mu\bar{\mu}$, $\tau\bar{\tau}$, $c\bar{c}$, $b\bar{b}$ and jets. The obtained results were consistent with the standard model predictions.

- $B_s^0 - \overline{B_s^0}$ mixing parameter was estimated from the measured asymmetry of b quarks combined with the other measurements of $B^0 - \overline{B^0}$ and $B_d^0 - \overline{B_d^0}$ mixing parameters. The hypothesis that $B_s^0 - \overline{B_s^0}$ mixing parameter is zero was excluded at 95% confidence level from this analysis.

- The existence of the triple gluon coupling was tested using the 4-jet events. The angular distribution was consistent with the non-Abelian

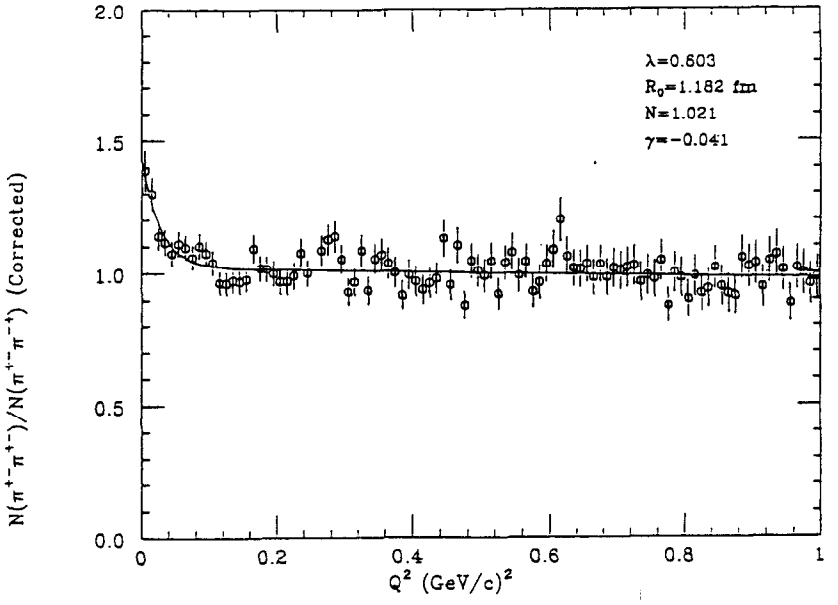

Figure 26: The ratio of the same and opposite charged particle pairs as a function of a square of the momentum difference obtained for the hadronic events sample of AMY.

(QCD) model which includes the triple gluon coupling. The Abelian model was excluded at 95% confidence level.

- The value of $\Lambda_{\overline{MS}}$ was determined using the Monte Carlo with the parton shower model based on the next-to-leading-log approximation.
- Various studies on the fragmentation were done. However, more statistics is necessary for further studies.

The author is grateful to the physicists of all TRISTAN experiments for providing the materials of this talk and for the fruitful discussions.

References

[1] (HRS): M.Derrick et al., Phys. Rev. **D31**(1985)2352; K.K.Gan et al., Phys. Lett. **B153**(1985)116; D.Bender et al., Phys. Rev **D30**(1984)515; (MAC): W.W.Ash et al., Phys Rev. Lett. **55**(1985)1831; E.Fernandez et al., Phys Rev. Lett. **54**(1985)1620; (MARK II): M.E.Levi et at., Phys. Rev. Lett. **51**(1983)1941; (CELLO): H.J.Behrend et al., Phys. Lett. **B114**(1982)282; H.J.Behrend et al., Phys. Lett. **B191**(1987)209; (JADE): W.Bartel et al., Z. Phys. **C30**(1986)371; W.Bartel et al., Phys. Lett. **B108**(1982)140; (MARK J): B.Adeva et al., Phys. Rev. Lett. **55**(1985)665; B.Adeva et al., Phys Rev. Lett. **48**(1982)1701; (PLUTO): C.Berger et al., Z. Phys **C27**(1985)341; C.Berger et al., Z. Phys **C28**(1985)1; (TASSO): R.Brandelik et al., Phys. Lett. **B110**(1982)173; M.Althoff et al., Z. Phys. **C22**(1984)13

[2] B.Adeva et al., L3-006(1990)

[3] C.Albajar et al., Phys. Lett. **B186**(1987)247

[4] W.T. Ford et al., Phys. Rev. **D36**(1987)1971

[5] A.J. Weir et al., Phys. Lett. **B240**(1990)289

[6] (JADE): W.Bartel et al., Phys. Lett. **B146**(1984)437; (TASSO): M.Althoff et al., Phys. Lett. **B146**(1984)443;C.Kiesling, in Proceeding of the 29th Moriond Conference, March, 1989; F.Ould-Saada, DESY report 88-177(1988); (MAC): H.R.Band et al, Phys. Lett. **B218**(1989)369; (HRS): C.R.Ng et al, ANL-HEP-PR-88-11; S.L.Wu, Nucl. Phys.**B** (Proc.Suppl.) 3(1988)

[7] H.Albrecht et al., Phys. Lett. **B192**(1987)245

[8] M.Artuso et al., Phys. Rev. Lett. **62**(1989)2233

[9] (VENUS): K.Abe et al., Phys. Lett. **B232**(1989)425; (AMY):D.Stuart et al., Phys. Rev. Lett. **64**(1990)983

[10] (AMY): I.H.Park et al., Phys. Rev. Lett. **62**(1989)1713; (TOPAZ): H.Iwasaki, Presented at Europhysics Conf. on High Energy Physics,

Madrid, Spain (1989); (VENUS): K.Abe et al., KEK-Preprint-90-62 (1990)

[11] M.Bengtsson and P.M.Zerwas, Phys. Lett. **B208**(1988)306

[12] M.Bengtsson, Z. Phys. **C42**(1989)75

[13] W.Bartel et al., DESY 86-086 (1986)

[14] F.Gutbrod, G.Kramer and G.Schierholz, Z. Phys. **C11**(1982)315

[15] R.K.Ellis et al., Nucl. Phys. **B178**(1981)421

[16] T.Sjöstrand, Comp. Phys. Comm **39**(1986)347; T.Sjöstrand and M.Bengtsson, Comp. Phys. Comm **43**(1987)367; T.Sjöstrand, JETSET7.2 (1989)

[17] D.Gottshalk and M.Shatz, Phys. Lett. **B150**(1985)452; preprints CALT-68-1172,CALT-68-1173

[18] R.Odorico, Nucl. Phys. **B172**(1980)157;G.C.Fox and S.Wolfram, Nucl. Phys. **B168**(1980)285; T.D.Gottshalk, Nucl. Phys. **B214**(1983)201, *ibid.* **B227**(1983)413

[19] K.Kato and T.Munehisa, CERN-TH-5719-90 (1990)

[20] (VENUS): K.Abe et al., Phys. Lett. **B240**(1990)232; (AMY):H.Sagawa et al., KEK preprint 90-67 (1990); (TOPAZ) private communication

[21] T.Kamae, Proc. of 24th Int. Conf. on High Energy Physics, Munich (1989)

[22] TRISTAN Theoretical Working Group (Kiyoshi Kato, et al.), KEK-87-5 (1987)

[23] S.Bethke et al., Z.Phys. **C43**(1989)325

[24] M.Suzuki, Phys. Lett. **B71**(1977)139; J.B.Bjorken, Phys. Rev. **D17**(1978)171

[25] C. Peterson et al., Phys. Rev. **D27**(1983)105

[26] G.Goldhabor et al., Phys. Rev. **120**(1960)300